catalysts

MDPI

Article

Experimental Design and Numerical Optimization of Photochemical Oxidation Removal of Tetracycline from Water Using Fe_3O_4-Supported Fruit Waste Activated Carbon

Manasik M. Nour [1], Maha A. Tony [2,3,*], Hossam A. Nabwey [1,*] and Shaaban M. Shaaban [4]

[1] College of Science and Humanities in Al-Kharj, Prince Sattam bin Abdulaziz University, Al-Kharj 11942, Saudi Arabia; m.mohamednour@psau.edu.sa
[2] Advanced Materials/Solar Energy and Environmental Sustainability (AMSEES) Laboratory, Basic Engineering Science Department, Faculty of Engineering, Menoufia University, Shebin El-Kom 32511, Egypt
[3] Planning & Construction of Smart Cities Program, Faculty of Engineering, Menoufia National University, Birket el Sab 32651, Egypt
[4] Center for Scientific Research and Entrepreneurship, Northern Border University, Arar 73213, Saudi Arabia; shaban.awdallah@nbu.edu.sa
* Correspondence: maha.shalaby@sh-eng.menofia.edu.eg (M.A.T.); h.mohamed@psau.edu.sa (H.A.N.)

Abstract: The ever-increasing importance of sustainable environmental remediation calls for academics' contribution to satisfy such a need. The *3R's* criteria of recover, recycle and reuse is designed to sustain the waste stream to produce a valuable product. In this regard, the circular economy looks to deliver banana peel waste as a photocatalyst for pharmaceutical effluent oxidation, which we investigated in this study. Banana peel waste is treated thermally and chemically then augmented with magnetite nanoparticles and labeled as ACBP-Fe_3O_4. The mixture is characterized through Scanning Electron Microscopy (SEM) and the composition of the composite material is attained by energy dispersive X-ray spectroscopy (EDX), and then introduced as a Fenton catalyst. The notable oxidation of tetracycline (TC), evaluated by TC removal and chemical Oxygen Demand (COD) oxidation tenancy, is achieved. The effectiveness of the operational parameters is also assessed and the most influenced parameters are optimized through numerical optimization based on a Response Surface Methodology (RSM) tool. The effects of initial pH value, ACBP-Fe_3O_4 and H_2O_2 concentrations on the oxidation efficiency of the Tetracycline were optimized at pH 6.6 and 350 mg/L and 43 g/L for H_2O_2 and ACBP-Fe_3O_4, respectively. Thermodynamics and kinetics were also studied and the experimental and model data revealed the reaction is spontaneous and exothermic in nature and follows the first-order reaction kinetics. Also, the thermodynamic results the reaction proceeds at a low energy barrier of 34.33 kJ mol^{-1}. Such a system introduces the role of engineers and academics for a sustainable world without a waste stream.

Keywords: tetracycline antibiotic; pharmaceutical effluent; banana peels; modified Fenton; activated carbon; magnetite

check for updates

Academic Editor: Tamara B. Ivetić

Received: 19 February 2025
Revised: 1 April 2025
Accepted: 2 April 2025
Published: 3 April 2025

Citation: Nour, M.M.; Tony, M.A.; Nabwey, H.A.; Shaaban, S.M. Experimental Design and Numerical Optimization of Photochemical Oxidation Removal of Tetracycline from Water Using Fe_3O_4-Supported Fruit Waste Activated Carbon. *Catalysts* **2025**, *15*, 351. https://doi.org/10.3390/catal15040351

Copyright: © 2025 by the authors. Licensee MDPI, Basel, Switzerland. This article is an open access article distributed under the terms and conditions of the Creative Commons Attribution (CC BY) license (https://creativecommons.org/licenses/by/4.0/).

1. Introduction

Today, one of the major concerns that the world is suffering from is the global water crisis, particularly experienced in most developing parts of the world [1]. Unskilled consumption and adaptation of natural water resources with a rapid rate of population and global industrialization increases the necessities of fresh water. But with the limited

availability of fresh water resources, about one billion human beings are categorized as having access to unsafe drinking water [2–5]. Furthermore, such statistics might be due to the fact that the world population is predicted to rise by ten billion by the year 2050. The successful adoption of a water roadmap is dependent on the availability of a sustainable method of water conservation. Cost and eco-friendly water management are the key. In order to cut down the cost of treatment, an industrial ecology approach is essential [6–9].

Currently, reports declare that there are no regulatory protocols for chemical chiral pollutants, including some drug residues that threaten human health due to the carcinogenic effects and economic losses linked to them [10,11]. Their presence in minimal concentrations in water as low as 1.0 ng/L might affect fish reproduction capability [12]. Generally, when pharmaceutical contaminants are present in the aquatic system, it causes drugs resistance in creatures [7]. Also, some pharmaceuticals and drug contaminants are converted onto receptor-specific chiral metabolites that trigger severe health outcomes [13–15].

Massive amounts of wastewater are generated from pharmaceutical discharge. Among the most applied medications, antibacterial drugs such as tetracycline (TC) are regarded as the most generally used [16–18]. Thus, this indicates that wastewater is highly contaminated with this drug. But tetracycline has become a severe warning to the environment due to its overuse by individuals [8]. On the other hand, this material possesses a weak ability to degrade, thereby accumulating along the food chain and causing toxicity to water and imbalance in the ecosystem. Thus, treating such discharge is a must. Effective selection of wastewater treatment is essential since ineffective wastewater treatments are among the main causes for the augmented antibiotic concentrations in water resources [5,19–22].

Various researchers [8,10,23,24] dealing with chiral pollutant removal facilities have introduced numerous research attempts. Such attempts include physical [25], chemical [26,27] and biological [28] treatments, for instance, filtration, coagulation, sedimentation, membrane separation, evaporation, reverse osmosis, ion exchange and adsorption [29–33]. However, such techniques harnessed the pollutants only by transferring them from one phase to another with no further mineralization [9,34]. Thus, advanced oxidation process (AOP) and photo-catalysis are gaining scientists' attention, due to their complete mineralization of such pollutants [35–38]. Fenton's oxidation technique, as one of the advanced oxidation processes, is gaining special interest due to its considerable high yield at low treatment costs for mineralizing undesirable chemicals and hazardous discharge [39].

Fenton's reaction is categorized by its unique photocatalytic activities and stable chemical structure [40–42]. However, such a reaction is not regarded as an ideal real applicable solution, since it possesses some limitations, such as the cost of the process due to the price of fresh chemical precursors as well as the essential nature of the reaction to work under acidic pH conditions, which requires excess treatment prior to the final disposal [14]. Thus, such issues make the application even more complicated [43,44]. Consequently, various advances have been outlined to overcome the drawbacks of the Fenton system reaction. The construction of a hetero-junction catalyst as a heterogeneous photocatalyst is required for adequate recovery facilities, and sustainable reuse is essential [45]. Nanoparticles, especially those that possess magnetic properties, are introduced as an excellent strategy for the option of recover, recycle and reuse facilities [46]. Thereby, the catalytic Fenton's oxidation is gaining researchers' interest.

On the other hand, with the major issues of solid waste, their elimination is gaining considerable attention [6]. Such waste material and their derivatives possess numerous functional groups that could be used for attacking the water contaminants and thereby eliminating them [6]. Biomass material waste valorization is most preferred recently due to its economic value and environmental friendliness [4,47–50]. In this regard, such substances have expanded the attention for pollutant adsorption from aqueous discharge [51]. Efficient

bio-waste materials have been tested, including potato peels, corn cob, sugarcane bagasse, rice husk, and banana peel, just to mention a few [52–54]. But this method has not been applied so far, to the authors' knowledge, as a photocatalyst in modified form.

The production of carbon from waste streams, namely activated carbon (AC)-based materials, has received great attention from researchers due the fact that it possesses reliable characteristics, including economic cost, large surface area and high catalytic activity. Furthermore, such materials become more reliable and economic when prepared from waste streams through chemical and physical treatments [55–59]. Additionally, their catalytic activity could be improved through modification and functionalization [57]. Amongst the chemical modifications, metal oxides are regarded as valuable materials due to their reliable efficiency in pollutants' remediation. Different waste biomass materials have been introduced as a source of AC, such as wood waste and lignin, rice husk and fruit waste [56–60]. Chemical activation techniques are essential to promote a carbonaceous structure of high porosity and large surface area, with various functional groups for numerous applications, especially wastewater treatment [57].

On the other hand, to date, numerous research articles have introduced the improvement of the photocatalytic characteristics of metal oxides by doping of varied inorganic and organic materials through simple, cost-effective techniques. These include wet chemical reduction, solvothermal facilities, hydrothermal techniques, wet chemical reduction, the sol-gel method and chemical deposition [55,58]. Also, their photocatalytic performances could be explored under visible, ultraviolet irradiance and/or sunlight radiation against toxic chemicals. Such materials include numerous nanostructured materials and their composites, such as carbon-based materials [59,61]. Such augmentation of metal oxides with AC-based materials could improve the surface catalytic activity, enduring photostability, and remarkable advantageous optical features [62–66]. Furthermore, the use of iron-based materials is superior, since they exhibit improved separation efficiency, contributing to sustainable use [59,67–69]. It makes the catalyst a suitable candidate for efficient utilization. Thus, combining metals oxides with carbon materials as a photocatalyst is a research topic.

Herein, activated carbon (AC) derived from waste banana peels modified with magnetite (ACBP@Fe_3O_4) was used as a photocatalyst for tetracycline (TC) removal from wastewater. ACBP@Fe_3O_4 nanoparticles were selected due to their cost-efficiency, magnetic properties, as well as the inclusion of various mixed elements that might help in the Fenton's oxidation. Also, it has the advantage of simple, reliable and cost-efficient preparation with a high yield. The optimum operating Fenton's parameters have been evaluated through experimental design using response surface methodology (RSM) techniques. The modified Fenton's reaction is a superior candidate to substitute the classical Fenton's type with no restrictions on the acidic pH and a recyclable environmentally benign catalyst facility.

2. Materials and Methods

2.1. Synthesis of Photocatalyst

Initially, the banana peels (BPs) were collected from a local fruit shop and the waste material was used to prepare the activated carbon (AC). Chopped and dried banana peels were used to prepare activated carbon. To prepare this type of activated material, initially, the peels were kept overnight at 70 °C. Thereafter, the dried material was first soaked in concentrated phosphoric acid (60%) for 12 h. Then, the soaked material was semi-carbonized in an electric oven to 200 °C (4 h). The semi-carbonized substance was cooled to room temperature then subjected to further heating and carbonized at 500 °C (2 h) for activation. The obtained material is labeled as ACBP. Afterwards, the attained material was successively washed with distilled water to remove any excess acid until exposure to a neutral pH. Finally, the obtained material was finally washed with NaOH solution (0.1 M),

followed by distilled washer washing. The produced powder was dried in an oven 105 °C (5 h) and ground in a mortar to obtain a fine powder.

On the other hand, a simple co-precipitation routine was applied for Fe_3O_4 nanoparticle preparation. The nanoparticles were prepared by mixing $Fe_2(SO_4)_3$ and $Fe(SO_4)$ in stoichiometric ratios with distilled water. Afterwards, a sodium hydroxide solution was added dropwise until the pH reached the alkaline range (about 11.0); in this stage the Fe_3O_4 nanoparticles were produced. Next, the liquid was elevated to 80 °C under continuous stirring. Subsequently, the material under went washing with distilled water to remove Na_2SO_4 and the excess NaOH and Na_2SO_4 until it reached neutral pH. The obtained substance was filtered and subjected to oven drying at 60 °C.

The powder activated carbon banana peel (ACBP) substance and the magnetite nanoparticles (Fe_3O_4) were then mixed in a ratio of 2:1 (ACBP: Fe_3O_4), respectively. This ratio was used according to a preliminary study and this is regarded as a cost-effective ratio. Then, the resultant material was labeled as ACBP-Fe_3O_4. This material was used as the source of Fenton's reaction as a modified Fenton's type. The graphical representation of the preparation steps is displayed in Figure 1.

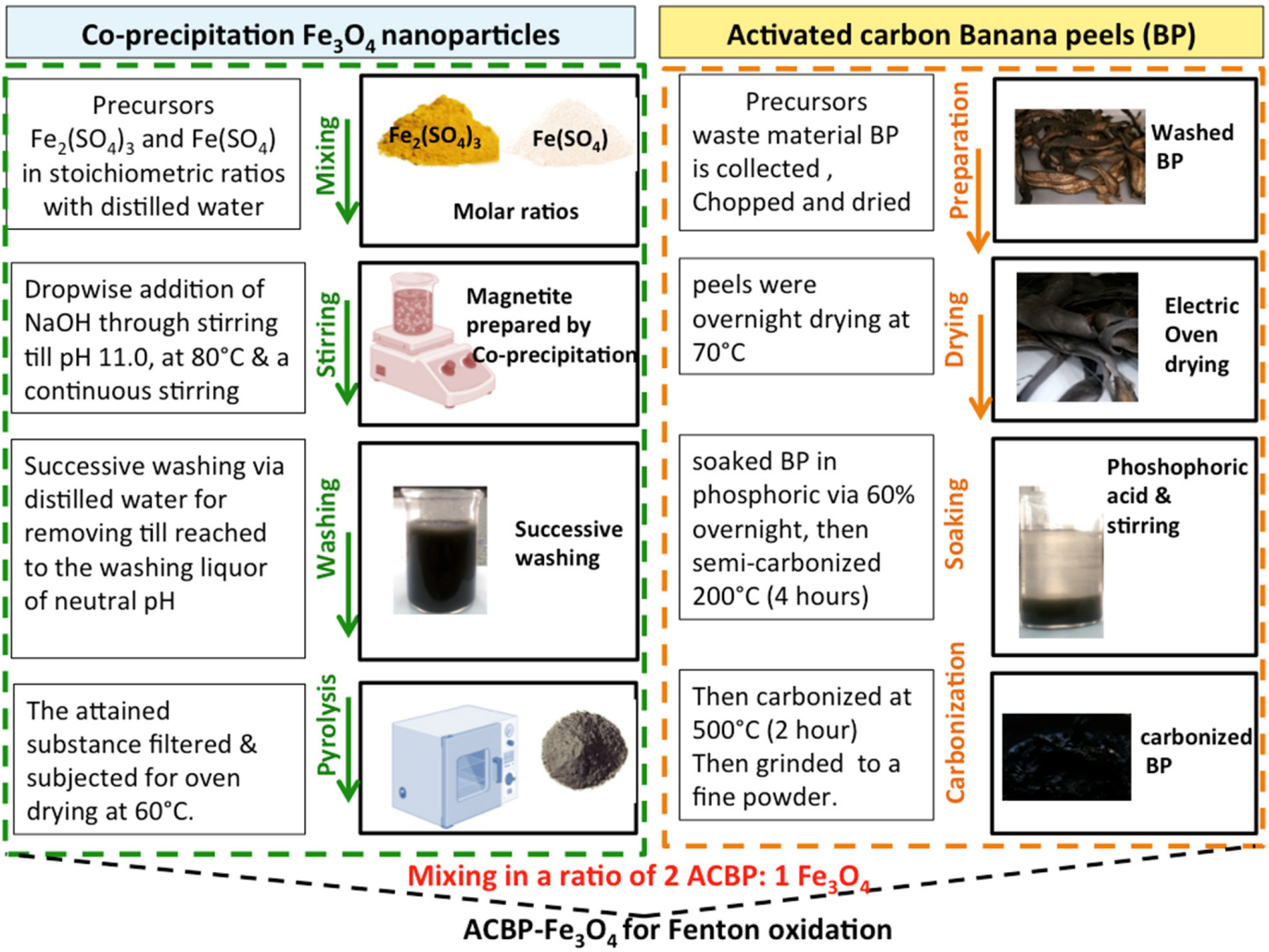


Figure 1. *Cont.*

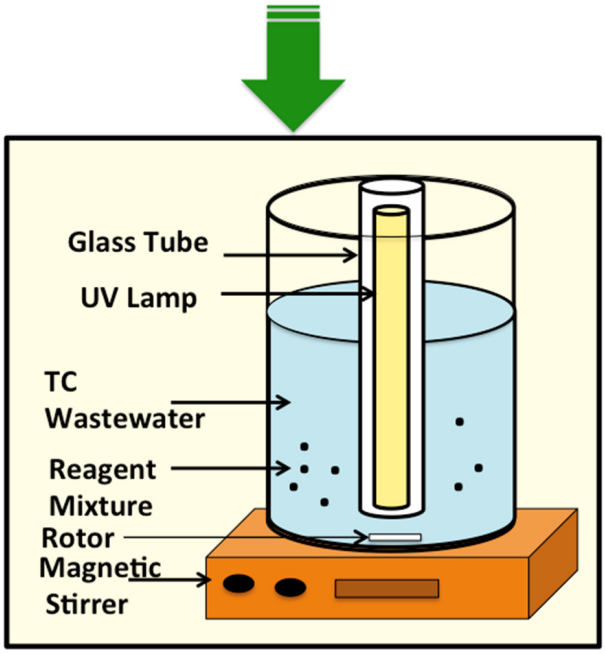


Figure 1. The graphical illustration of material preparation steps and treatment technique.

2.2. Characterization of the Photocatalyst

The structure of the prepared sample is characterized by X-ray diffraction (XRD) measurements performed on a Bruker-Nonius Kappa CCD diffractometer (Bruker, Billerica, MA, USA) with CuKα radiation source (λ = 1.5406 Å).

The morphology of the prepared ACBP-Fe_3O_4 substance was evaluated and imaged by field-emission scanning electron microscope (SEM) (FE-SEM, Quanta FEG 250, Madrid, Spain). Typical magnifications used were x8000 and x60,000. This measurement was accompanied by energy dispersive X-ray spectroscopy (EDX). The principal elements' contents in the ACBP-Fe_3O_4 were examined by energy dispersive spectrum. Also, the BET surface area of the ACBP-Fe_3O_4 material was determined using a nitrogen gas sorption analyzer (Quantachrome, Model: TouchWin version 1.21, Sydeny, Austria).

2.3. Methodology

A lab-scale batch mode setup is applied as an experimental test using a 12 W UV lamp. The lamp is a glass sleeve inside the reactor, immersed in a glass container. Initially, ACBP-Fe_3O_4 is added to 100 mL of wastewater solution, where the pH is first adjusted when required. Afterwards, the reaction is initiated by adding H_2O_2 reagent at a certain concentrations. H_2O_2 (30% *w*/*v*) was used and applied in the reaction medium as the initiator of the modified Fenton oxidation reaction. The pH of the tetracycline antibiotic-containing aqueous solution was recorded at 6.5 and then was adjusted, if needed, to the required values using H_2SO_4 or NaOH (all supplied by Sigma-Aldrich, St. Louis, MO, USA).

The reagents are immersed in the aqueous solution, then the solution is poured into the photo-chemical reactor. After 10 min of reaction time treatment, the substrate of the treated wastewater samples is subjected to TC and COD removal analysis.

The graphical illustration of the treatment technique augmented with the material the preparation steps is exhibited in Figure 1.

2.4. Analysis

A UV-vis spectrophotometer (Unico UV-2100 spectrophotometer, Dayton, NJ, USA) was used to evaluate the residual TC concentration at set time intervals. Prior to measurements being made, the ACBPs augmented with Fe_3O_4 catalyst were exposed for separation through the

use of a micro-filter (0.45 μm). The samples' pH was adjusted when needed by using a digital pH meter (Model AD1030, Adwa instrument, Szeged, Hungary). Also, the measurement of its chemical oxygen demand (COD) following standard methods (APHA, 1998) was carried out.

2.5. Box–Behnken Factorial Design

An experimental design model and statistical data analysis are applied for estimating the optimum effect of the operating parameters for the applied modified ACBP-Fe_3O_4-based photo-Fenton system. Response surface methodological analysis (RSM) related to the experimental factorial design is mostly applied to optimize the multi-varied response. The Box–Behnken experimental factorial design model was selected to represent the data. A 3-factor design, codded as –1, 0 and 1, was projected for each selected most influenced operational parameter, including H_2O_2 dose, ACBP augmented with Fe_3O_4 catalyst dose and the starting pH value. Therefore, the total design matrix was proposed as fifteen runs through the application of SA (Statistical Analysis) Software (SAS 9.4). A mathematical model was established and then the link between the selected predicted and experimental response and the 3 independent parameters was projected, referring to the following second-order polynomial model equation:

$$f = \beta_o + \sum \beta_i X_i + \sum \beta_{ii} X_i^2 + \sum \beta_{ij} X_i X_j \quad (1)$$

where f is the predicted values of the response of the TC oxidation efficacy (%); β_o, β_i, β_2 and β_{ii} are the model coefficients and X_i and X_j are the independent variables (SAS 9.4).

Mathematica software (version V 5.2) was applied to evaluate the optimized values of the coded independent factors for the interactive variables.

2.6. Statistical Analysis

For the purpose of obtaining the statistical significance of the proposed model, the data produced from the RSM design are statistically analyzed using analyses of variance (ANOVA) to estimate the significant difference ($p < 0.05$) between the same experimental group at different times and between the different experimental groups in the same experimental period. The statistical analysis was performed using Statistical Analysis software SAS (1990, ver 9.4).

3. Results and Discussion

3.1. Characterization of ACBP-Fe_3O_4

Figure 2 shows the XRD diffractogram of the ACBP-Fe_3O_4 substance showing two wide peaks (at 24° and 43°), which correspond to the (002) and (100) reflections planes of graphite (Pattern Diffraction File database, PDF 41–1487), respectively [70]. Furthermore, this XRD pattern verified the coexistence of Fe_3O_4 and ACBP in the substance. This is verified with the characteristic peaks of the magnetite. The peaks at 2θ values of 30° (220), 35° (311), 43° (400), 57° (511), and 63° (440) are in agreement with the standard XRD data for the pure cubic spine crystal structure of magnetite (JCPDS No. 89-4319) [71,72].

The physical morphology of the prepared ACBP-Fe_3O_4 material particles is exhibited in Figure 3. The figure displays the SEM images, which reveal that ACBP-Fe_3O_4 possesses a heterogeneous structure with non-uniform shape mixture. Consequently, the ACBP-Fe_3O_4 material retains its uneven structure. Also, the porous structure of the prepared ACBP-Fe_3O_4 is verified by its BET surface area, which signifies 428 m^2/g BET surface area.

Elemental analysis of ACBP-Fe_3O_4 material as determined by EDX is demonstrated in Table 1. The calcined banana peel powder augmented with Fe_3O_4 contains the main Fe and C components, along with Cu and Zn, with the presence of small amounts of S, Cr, N and Ni. The augmentation of magnetite with the calcined material is reflected in

the composition of the catalyst produced. Also, carbon is reflected in the biomass waste pyrolysis. The presence of these elements, along with Cu and Zn, supports the material's potential role as a photocatalyst.

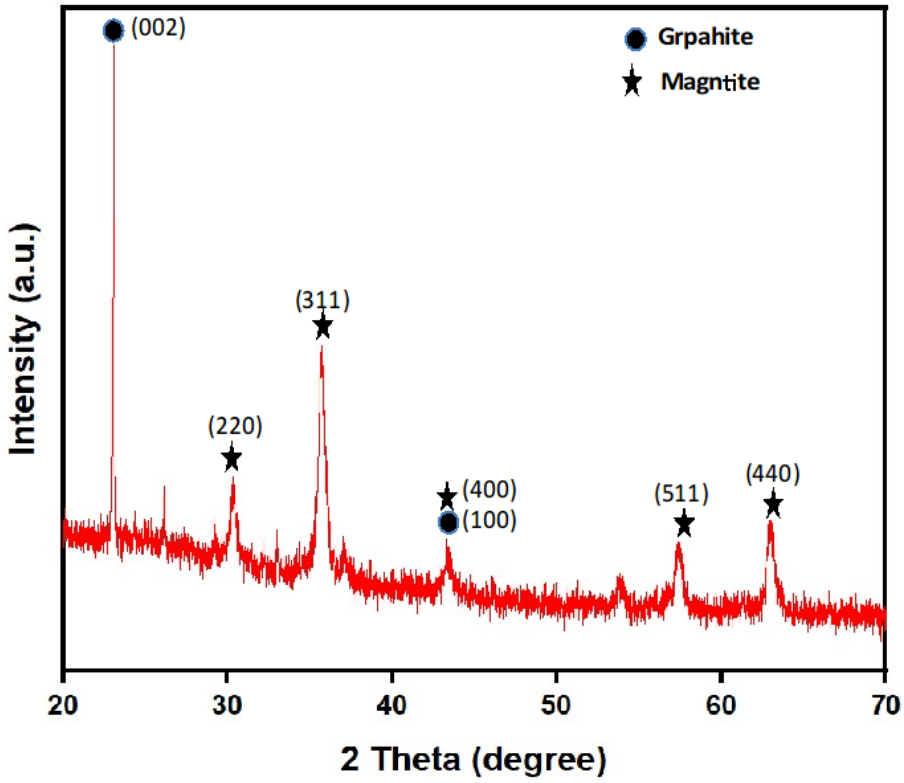


Figure 2. XRD pattern of the prepared ACBP-Fe_3O_4 catalyst.

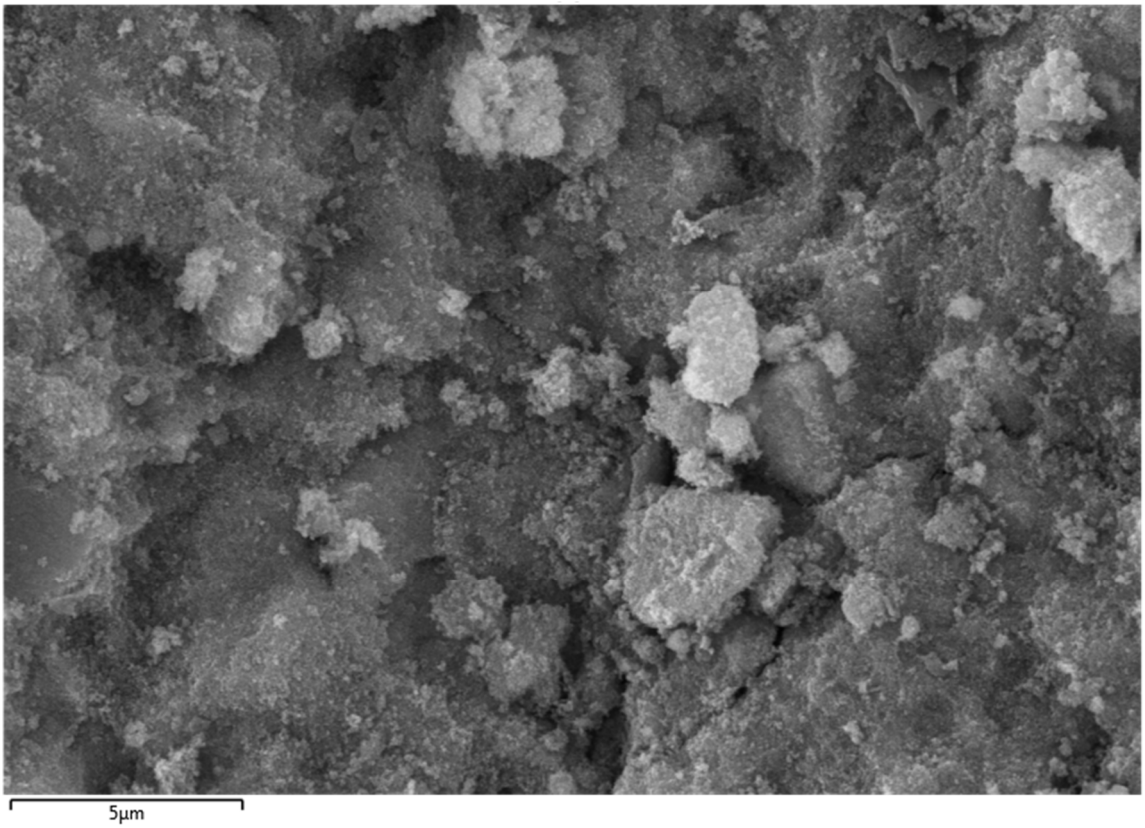


Figure 3. SEM images of activated banana peel samples augmented with magnetite nanoparticles.

Table 1. Chemical composition of ACBP-Fe_3O_4 inferred by EDX.

Element	C	N	S	Cr	Fe	Ni	Cu	Zn	Total
Weight %	10.56	0.55	0.04	0.06	87.96	0.26	0.42	0.15	100

3.2. Photochemical Oxidation

3.2.1. Effect of Oxidation Time and Different Oxidation Systems

Primarily, to examine the optimum introduced modified photo-Fenton's oxidation time for both tetracycline (TC) and chemical oxygen demand (COD) removals (% from contaminated aqueous effluent for further following tests), experiments were executed at various oxidation times, and both values of TC and COD oxidation efficiency rates were evaluated. Also, for the object of comparison, the modified Fenton's reaction system is compared with the solo oxidation systems of ACBP/UV, ACBP, ACBP-Fe_3O_4/UV or H_2O_2/UV. The modified Fenton's reagents were selected as 40 mg/L for ACBP and 400 mg/L for hydrogen peroxide reagent (H_2O_2), respectively. The data exhibited in Figure 4A,B verified that the values of TC and COD for all studied systems declined as the reaction time increased. For the modified Fenton's reaction system, a rapid oxidation rate was first detected within the initial 10 min of irradiance time. Then, a steady oxidation rate was observed for the next 20 min. The total TC and COD removal values reached 95% and 93%, respectively. However, for the solo and magnetite-free systems, the COD removal values reached only 25, 33 and 66%, for ACBP/UV, H_2O_2/UV and ACBP/H_2O_2/UV, respectively. However, for the dark ACBP, the oxidation reached only 13% of COD reduction and 18% for TC removal. Also, the TC removal values declined from 95% to 33, 42 and 78% for the magnetite-free systems (ACBP/UV, H_2O_2/UV and ACBP/H_2O_2/UV, respectively). Thus, the investigation confirms the role of the combined Fenton system in the treatment.

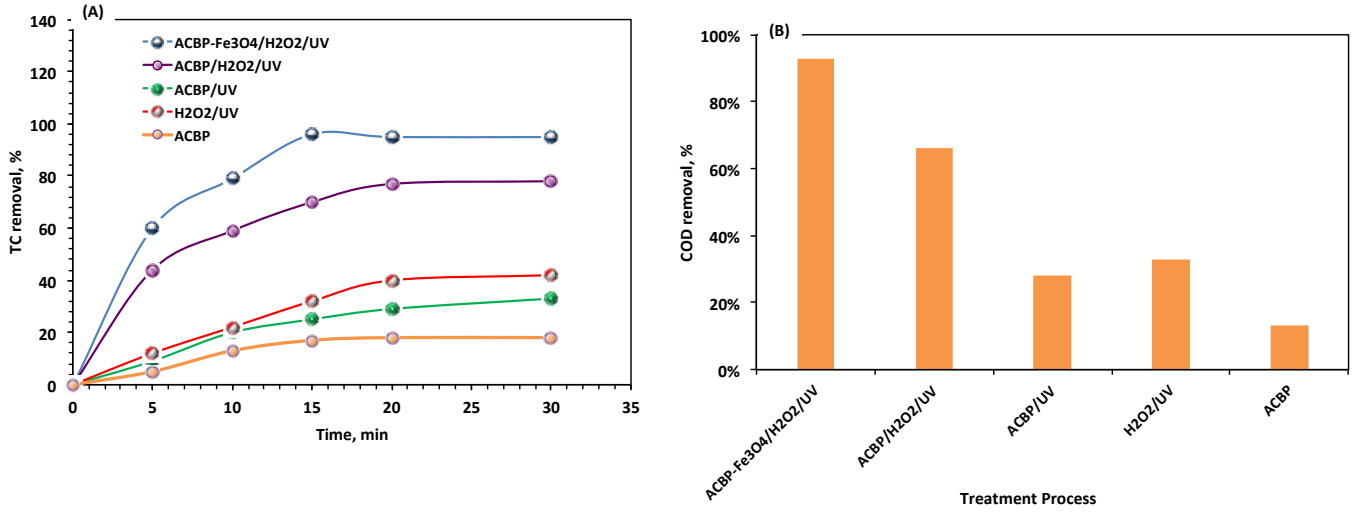


Figure 4. Comparison of reaction time effectiveness on different oxidation activity systems: (**A**) the change in TC with the reaction time; (**B**) the change in COD with the reaction time.

The oxidation rate detected via TC and COD deduction is attributed to the establishment of the most reactive oxidation species of hydroxyl radicals (·OH) in the case of the Fenton oxidation reaction. These hydroxyl OH radicals possess viable oxidation ability, thereby attacking the tetracycline in the contaminated water and mineralizing it. Still, the solo system exhibited some oxidation capability, but at a low reduction rate. This result confirms the existence of the Fenton's reaction in oxidizing the pollutants. This might be linked to the extra ·OH radicals' production rate in the case of the combination of hydrogen peroxide and catalyst.

3.2.2. Effect of Fenton's Reagent Parameters

Effect of Reaction pH

In general, the Fenton oxidation system is too sensitive to the operating pH conditions due to the fact that this oxidation reaction system is particularly determined by the generation of ·OH radicals. As previously stated in the cited data, pH plays a significant role in the Fenton oxidation reaction, since the Fenton reaction has a preferred optimum pH value that sharply affects the OH radicals' production. Generally, .OH radicals play the role of the workhorse of H_2O_2 augmented with the catalyst oxidation systems. Consequently, iron speciation and hydrogen peroxide decomposition are affected by the oxidation reaction. Furthermore, the oxidizing power of hydroxyl radicals declines under high-pH conditions.

In this regard, experiments have been conducted in various pH conditions, and the results are displayed in Figure 5A,B. The data indicate that decreasing the pH to acidic conditions is not favorable. The highest TC and COD removal values correspond to pH 6.5, which is the natural pH of the wastewater without further adjustment. The TC and COD are 98 and 94%, respectively. But a further increase in pH into alkaline conditions is not favorable and results in a decline in the oxidation rate. TC oxidation strongly reduces as ACBP catalyst complexes might precipitate in the aqueous mixture instead of generating the OH radicals' species in the aqueous reaction medium for the oxidation reaction. Therefore, the reaction includes the organometallic complex. On the other hand, the production of hydroxyl (·OH) radicals under mild pH conditions was maximized. These data verify the upsurge in the TC removal at the natural pH value, and the most noteworthy oxidation rate for both TC and COD was attained at a pH value of 6.5. Also, it is worth mentioning that the acidic pH conditions also oxidize TC to 62%, which is not too high for the natural pH. It is essential to mention that this treatment overcomes the drawback of Fenton's limitation to the acidic pH [12]. This could be attributed to the multi-element source of the Fenton's catalyst, and as such, might work under various pH conditions. Also, the unsuitable pH further scavenges the hydroxyl radicals' effect and precipitates the elements in the reaction rather than reacting with hydrogen peroxide to generate OH radicals [40]. Furthermore, the presence of activated carbon in this treatment further treats the wastewater. These data indicate that the modified Fenton reaction based on ACBP-Fe_3O_4 was a superior catalyst for modified Fenton's reagent to treat pharmaceutical discharge contaminated with TC due to the fact that it delivers great oxidation and elimination of organics at low cost, as well as eradicating the fruit waste.

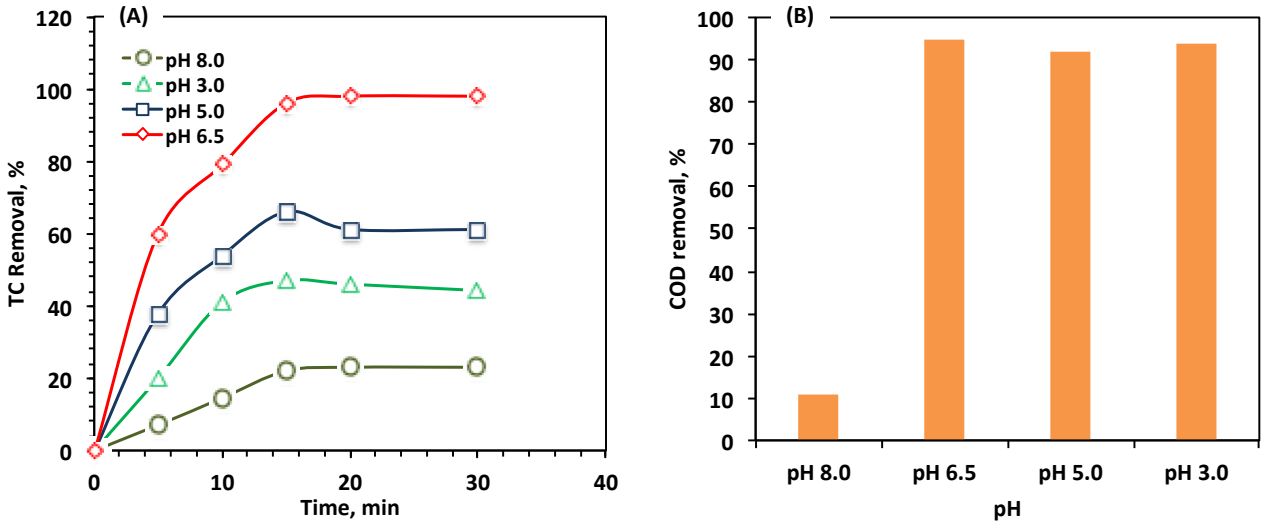


Figure 5. Effect of pH on the (**A**) TC removal and (**B**) COD reduction for the modified Fenton oxidation system.

Effect of H_2O_2 Reagent

The existence of .OH radicals and oxygen in the reaction medium is mainly related to the occurrence of H_2O_2. From this point of view, the influence of the concentration of hydrogen peroxide on the modified ACBP-based Fenton's reaction was investigated by altering the initial hydrogen peroxide dose from 100 to 800 mg/L at natural pH (6.5) and ACBP-Fe_3O_4 of 40 mg/L.

Figure 6A,B exemplify the TC and COD removal efficiency, respectively. The oxidation efficacy is improved by the elevation in the hydrogen peroxide reagent from 100 to 400 mg/L, improving the %COD removal (from 55 to 95%) and %TC reduction (from 47 to 98%). This could be related to the production of hydroxyl (·OH) radicals, which are chiefly responsible for the oxidation process. Nevertheless, the excess upsurge in H_2O_2 dose above the concentration limit results in a decline in both %COD and %TC elimination. The excess H_2O_2 leads to the auto-decomposition of the hydrogen peroxide reagent into O_2 and H_2O, which could illustrate this. Also, the resultant OH radicals in the reaction medium further recombine with each other. Hence, extra H_2O_2 beyond the optimal limit serves as a ·OH radical scavenger rather than a generator. Our examination verifies the role of an optimum dose of hydrogen peroxide in generating hydroxyl (·OH) radicals [12,44]. These data are in agreement with those previously reported in the cited literature regarding the elimination of pollutants from wastewater by the Fenton's reaction oxidation system.

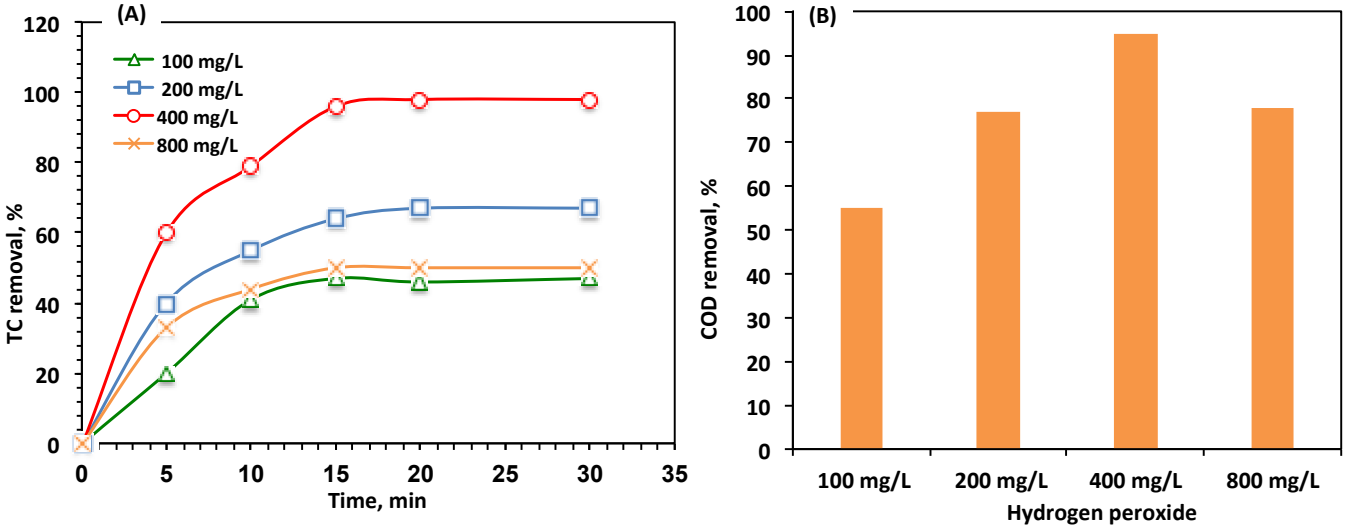


Figure 6. Effect of hydrogen peroxide dose on the (**A**) TC removal and (**B**) COD reduction for the modified Fenton oxidation system.

Effect of Catalyst "ACBP-Fe_3O_4" Reagent

Besides the initial dosing of H_2O_2 reagent, the initial catalyst dose limit is also important. The catalyst catalyzes the production of hydroxyl radicals from the hydrogen peroxide reagent. Hence, the production of (hydroxyl ·OH) radicals is exaggerated by the ACBP-Fe_3O_4 catalyst dose, as displayed in Figure 7A,B. ACBP catalyst addition into the reaction was conducted at different ACBP-Fe_3O_4 concentrations in the range from 10 to 80 mg/L. The pH of 6.5 and 400 mg/L of hydrogen peroxide dose were maintained at their constant optimal levels. As exhibited in Figure 7A,B, the increase in ACBP concentration has a favorable influence on both the TC and COD oxidation efficiency until a specific critical value limit of 40 mg/L. But the oxidation rate was produced with the elevation in the ACBP-Fe_3O_4 dose above this 40 mg/L concentration. Therefore, ACBP-Fe_3O_4 species with various elements are a limiting reagent in the modified Fenton reaction system and may exist at much lower concentrations than hydrogen peroxide reagent. This

examination of the use of minimal catalyst concentration validates the advantage of the modified Fenton method in diminishing the final sludge generated after the oxidation of wastewater. Villegas-Guzmana et al. [14] reported this data trend in previous research in treating contaminated aqueous effluent with organics using the Fenton system.

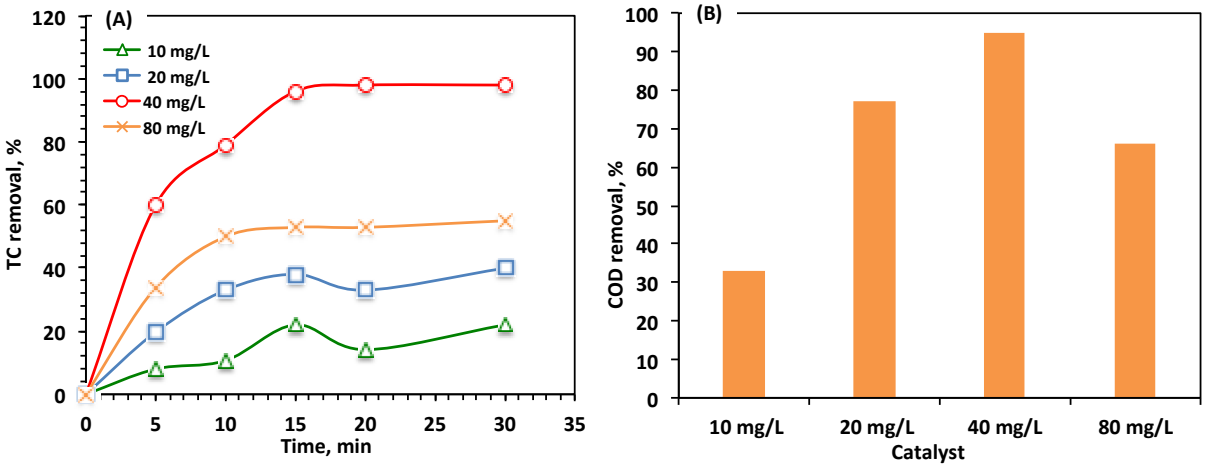


Figure 7. Effect of ACBP-Fe_3O_4 catalyst dose on the (**A**) TC removal and (**B**) COD reduction for the modified Fenton oxidation system.

3.3. Numerical Optimization

3.3.1. Model Establishment

Numerical optimization is applied to assess and optimize the ACBP-based Fenton's reagent parameters based on Box–Behnken factorial design as a response surface methodology (RSM) tool. The design is applied to explore the influence of the 3 effective modified Fenton's reaction operating variables, namely H_2O_2, ACBP-Fe_3O_4 concentrations and pH. According to the preliminary experiments, the range as well levels of the experimental domain design were determined, and these values are listed in Table 2, including their coded and corresponding natural parameter levels. The presentation of the modified Fenton system was assessed by the TC removal, in terms of %, as the predicted and experimental response.

Table 2. Design boundaries of the experimental domain with their spacing levels in their coded and uncoded values.

Variable	Symbols		Range and Levels		
	Natural	Coded	−1	0	1
H_2O_2 (mg/L)	x_1	X_1	350	400	450
ACBP-Fe_3O_4 (mg/L)	x_2	X_2	35	40	45
pH	x_3	X_3	6.0	6.5	7.0

A total of 15 experimental runs are displayed in Table 3, in agreement with the design model in terms of the predicted and natural (uncoded) values of their consistent predicted and experimental responses. The data exhibited in Table 4 are the triplicates of the experimental runs. Regarding the experimental data, a second-order polynomial equation of the predicted model was projected to examine the correspondence of the response function.

Consequently, the quadratic polynomial equation in the terminologies of the coded parameters levels is exhibited according to the following equation:

$$f = 44.33 - 24.87\ X_1 + 7.54\ X_2 + 3.62\ X_3 + 0.45X_1^2 - 7.13X_1X_2 + 0.75X_1X_3 + 3.79X_2^2 - 1.52X_2X_3 - 4.54X_3^2 \quad (2)$$

Table 3. Coded and actual Box–Behnken design of experiments and the predicted and experimental response.

Run No.	Codified Variables			Natural Variables			Response (%TC Removal)	
	X_1	X_2	X_3	x_1	x_2	x_3	Experimental	Predicted
1	−1	−1	0	35	350	6.5	61	59
2	−1	1	0	35	450	6.5	94	88
3	1	−1	0	45	350	6.5	17	23
4	1	1	0	45	450	6.5	22	24
5	0	−1	−1	40	350	6.0	32	31
6	0	−1	1	40	350	7.0	44	42
7	0	1	−1	40	450	6.0	46	49
8	0	1	1	40	450	7.0	52	53
9	−1	0	−1	35	400	6.0	59	62
10	1	0	−1	45	400	6.0	16	12
11	−1	0	1	35	400	7.0	63	68
12	1	0	1	45	400	7.0	23	20
13	0	0	0	40	400	6.5	44	44
14	0	0	0	40	400	6.5	44	44
15	0	0	0	40	400	6.5	45	44

Table 4. ANOVA test results for the response surface model for TC removal by modified ACBP-Fenton system.

Source	Degree of Freedom (*DF*)	Sum of Squares (*SS*)	Mean Squares (*MS*)	Fisher (*F*-Value)	Probability (*p*-Value)
Model	9	5850.817	650.0907	18.58287	0.002485
Linear	3	5505.25	5505.25	157.367772	0.15941
Square	3	199.025641	199.025641	5.689156	1.761538
Interaction	3	135.9359	135.9359	3.885733	1.115889
Error	5	174.9167	34.98333		
Total	14	6025.733			
			R^2: 97%		

3.3.2. ANOVA Test

ANOVA (analysis of variance) was selected to assess the appropriate fit of the experimental model (Table 4). In general, the model is coherent, since the probability (*p*-value) is small, whereas the large *F* (Fisher-test) consists of large values, with a correlation coefficient that should be >0.8. The data displayed in Table 4 reveal the fitness of the model, with a confidence level assessed by the regression coefficient value (R^2 = 97%), with a minimal model probability value (*p*-value < 0.05) [14]. The proposed model is considered as highly suggestive with a low probability value.

Analysis of variance (ANOVA) data (Table 4) reveal that the proposed model possess a *p*-value of 0.0024, which confirms the model validity. Furthermore, the 'lack-of-fit' *F*-value for the response of the TC removal percent predicted by the proposed model was applied to check its validity. The *F*-value of 18.58 suggests the effectiveness of the model in fitting the data with good consistency. Moreover, the ANOVA of the data shows a high significance between the experimental and predicted TC removal, which verifies the goodness-of-fit of the model for the results.

3.3.3. Graphical Illustration

To further illustrate the design, consequently, a response 3-D surface and 2-D contour graphical illustrations, obtained based on the experimental results, were used to explain the 3 interacting parameters and their influences on the TC reduction efficacy using MATLAB R2017a software. Figure 8A,C,E shows the interaction outcome between the two independent variables and the response (% TC removal). The graphs demonstrate that TC elimination efficacy improved as both ACBP-Fe_3O_4 and H_2O_2 reagents increased up to a certain limit,

as displayed in Figure 8. Nevertheless, the extra upsurge in the reagent concentrations beyond the optimum region resulted in a decrease in the TC removal proficiency. Afterwards, extra ·OH radicals affect the ACBP precipitation because they are converted to OH ions. Consequently, the precipitated ACBP-Fe_3O_4 contributes to a decrease in the concentration of ACBP in the system, leading to an overall decrease in the TC reduction efficacy.

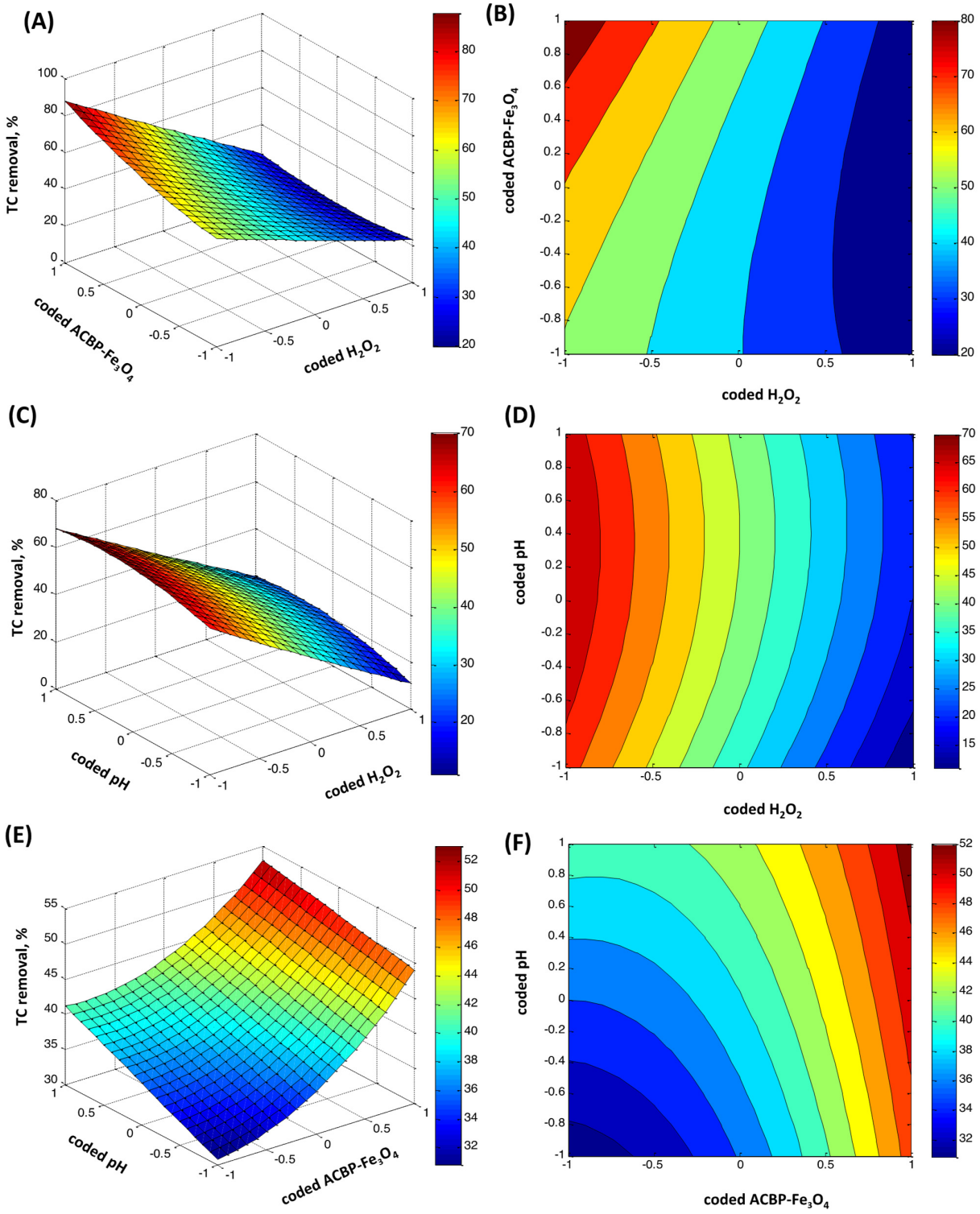


Figure 8. Box–Behnken design graphical illustration for TC removal from aqueous solution using ACBP-Fe_3O_4 -based Fenton system: (**A**) 3-D surface and (**B**) 2-D contour plot of coded H_2O_2 and ACBP-Fe_3O_4, (**C**) 3-D surface and (**D**) 2-D contour plot of coded H_2O_2 and pH and (**E**) 3-D surface and (**F**) 2-D contour plot of coded ACBP-Fe_3O_4 and pH.

Likewise, at constant H_2O_2 dose, a significant TC removal efficiency upsurge was obtained with the elevation of both ACBP-Fe_3O_4 dose and pH value. The plots in Figure 8E,F reveal that there is an optimum range for pH and ACBP-Fe_3O_4 dose. But beyond the suggested range, a decline in the TC removal effectiveness is noted. The pH of the aqueous solution had a terminal influence on the Fenton's reaction system that affects both the production of OH radicals and the amount of catalyst in the mixture. These data might be due to the fact that at a higher pH value, the possibility of H_2O_2 decay is higher. Consequently, the results validate higher TC removal efficiency under acidic pH conditions. Furthermore, high pH values help ACBP ions to trigger the ferric-hydro-complex, and this produces the overall oxidation efficiency.

Further, the predicted and experimental values of responses are also compared according to Figure 9. The predicted values of response are obtained from a quadratic model using SAS software Ver 9.4. The response functions with the determined coefficients for TC removals (%) are investigated based on Equation (2). As displayed in Figure 9, a high correlation is achieved between the predicted and experimental values (R^2: 98%).

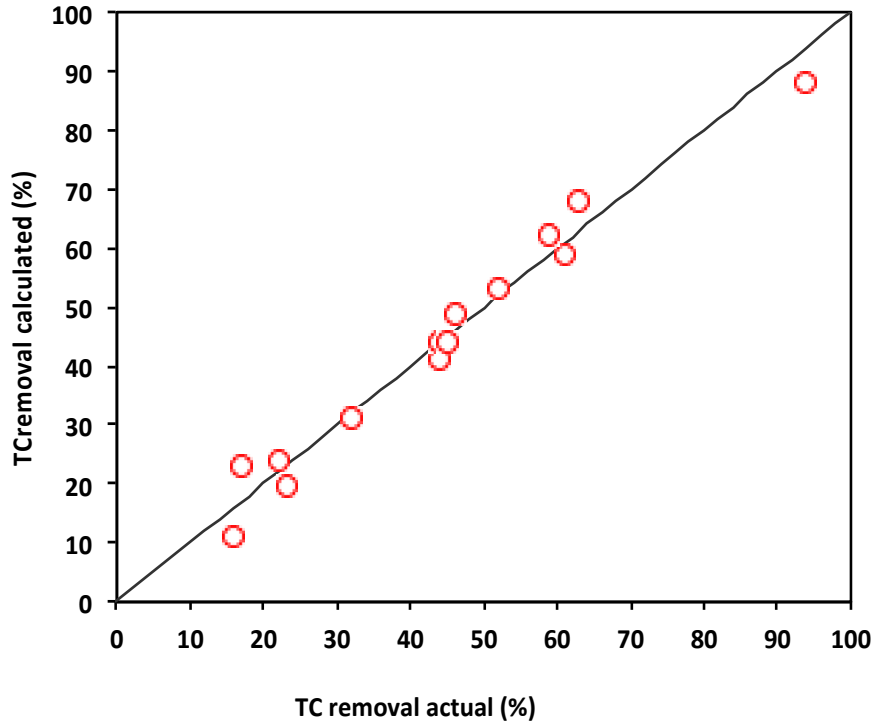


Figure 9. Graphical illustration of Box–Behnken design for actual and predicated regression plot responses.

3.3.4. Model Verification

Ultimately, for the purpose of verifying the predicted model and the proposed statistically estimated values (H_2O_2 350 mg/L, ACBP-Fe_3O_4 43 mg/L and pH 6.6), an additional three replicates were conducted and the experimental TC removal response values were compared with those projected and proposed by the suggested model (98% TC removal). After 30 min of irradiance time, the experimental TC removal reached 99%, which is close to the estimated value using the Box–Behnken design. Consequently, those results confirm the significance of the Box–Behnken design based on RSM for locating the optimum operating parameters for the oxidation of organics through the ACBP-based Fenton system.

3.4. Study of Temperature on Reaction Kinetics and Thermodynamics

For the purpose of evaluating the operating temperature effect on TC oxidation, the process is conducted at various operational temperatures and the results are displayed in

Figure 7. Modified Fenton reagent doses are introduced to the jar test at constant values of ACBP-Fe_3O_4 (40 mg/L) and hydrogen peroxide (400 mg/L) at a natural pH value of 6.5.

As presented in Figure 10A,B, both TC and COD decline in their rates as the temperature increases from room temperature (28 °C) to 60 °C. Thus, a decline in the tetracycline oxidation is achieved with the elevation of temperature. TC removal decreased from 98 to 49% and COD removal also declined from 95 to 55% with the temperature increase from 28 to 60 °C. This could be attributed to the decay rate of the hydrogen peroxide reagent into O_2 and H_2O that happened at a high rate at elevated temperatures. Consequently, H_2O_2 acts as a free radical oxidation scavenger rather than a radical creator. Thus, the result is a decrease in the OH radical generation, which initiates tetracycline oxidation [43]. This oxidation tendency is clearly in agreement with that reported in the previously cited work in the literature for wastewater treatment with Fenton's reaction [12,33,54].

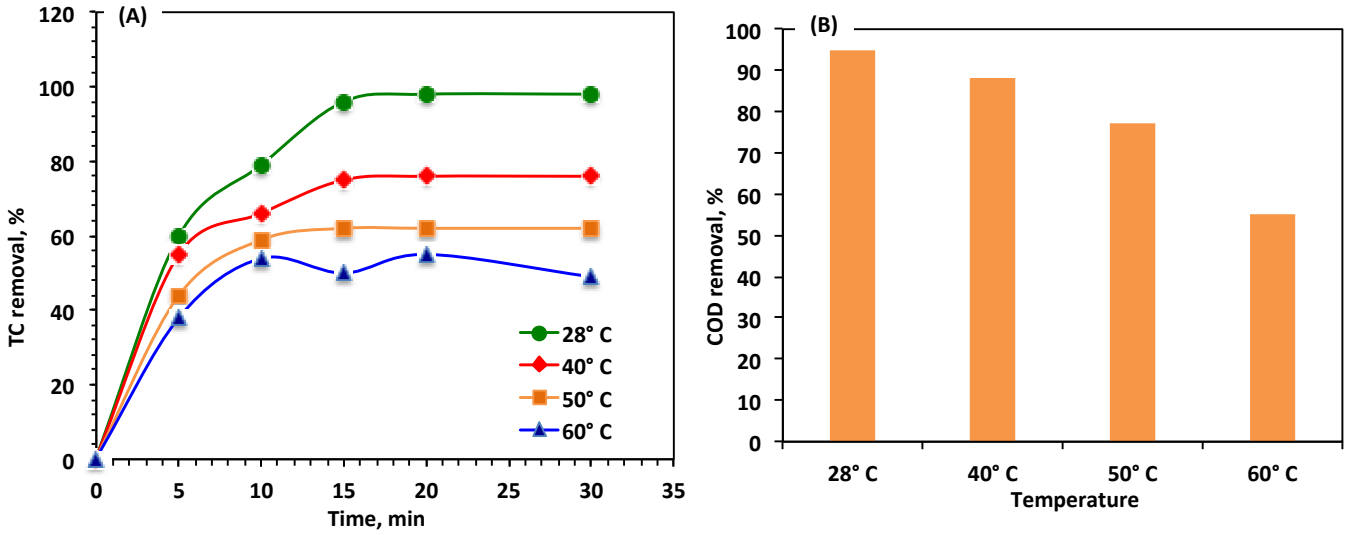


Figure 10. Effect of temperature on the (**A**) TC removal and (**B**) COD reduction of modified Fenton oxidation system.

To obtain a thorough understanding of the modified Fenton oxidation system based on ACBP-Fe_3O_4/H_2O_2 under mild pH conditions, kinetic modeling is applied to realize a practical real-life facility for application. These data act as a guide to further investigate the varied mechanisms of the oxidation process. To achieving appropriate kinetic modeling, the optimum operational variables, economic investigation, system control and also a scale-up design facility should be assessed. In this regard, a set of kinetic models is applied based on varied operating temperatures. According to the equations of the zero, pseudo-first- and second-order reaction rates, respectively, displayed in Table 5, which sets the relationship between different initial concentrations and time, the models are applied. The data tabulated in Table 5 represent the kinetic rate constants and the reaction half-life ($t_{1/2}$) of the three applied models.

Notably, from Table 5, the assessment for all the proposed models is based on the regression coefficient (R^2) values. According to the data of R^2 values exhibited in Table 5, the first order is the most appropriate in terms of fitting the experimental data. Also, the half-reaction time ($t_{1/2}$) is shown to be increased with the elevation of temperature for tetracycline oxidation. This trend might be linked to the fact that the overall amount of hydroxyl radicals is reduced with the increase in temperature. Furthermore, this could be explained by the fact that increasing the temperature of the aqueous solution hindered the catalytic activity of ACBP-magnetite to adsorb TC, since the catalyst surface deteriorates under elevated temperature. This is due to the desiccation of hydrogen peroxide into oxy-

gen and water instead of producing hydroxyl radicals [61,62]. Various researchers [63,64] previously reported the experimental evidence for the dependence of catalytic oxidation on temperature. Thus, the overall oxidation reaction yield declines [45]. Therefore, the effect of temperature on tetracycline oxidation through the novel modified ACBP-Fe_3O_4/H_2O_2 composite-based Fenton catalyst follows first-order reaction kinetics. First-order reaction kinetics indicate that the rate of reaction is directly proportional to the concentration of reactants. Also, according to the values of the rate constant k_1 displayed in Table 5, the rate constant depends on the reaction temperature, thereby affecting the rate of TC oxidation. To sum up, the half-life time is related to the rate constant k_1.

Table 5. Kinetic parameters of TC pharmaceutical wastewater treatment by modified Fenton under various temperatures *.

T, °C	Zero-Order Reaction Kinetics Model			First-Order Reaction Kinetics Model			Second-Order Reaction Kinetics Model		
	$C_t=C_o-k_o t$			$C_t=C_o-e^{k_1 t}$			$\left(\frac{1}{C_t}\right)=\left(\frac{1}{C_0}\right)-k_2 t$		
	k_o, min^{-1}	R^2	$t_{1/2}$, min	k_1, min^{-1}	R^2	$t_{1/2}$, min	k_2, L mg^{-1} min^{-1}	R^2	$t_{1/2}$, min
28	0.464(±0.121)	83	10.7758	0.047(±0.015)	0.97	3.3804	0.241(±0.064)	0.82	0.01085
40	0.344(±0.117)	74	14.5348	0.081(±0.017)	0.92	8.5556	0.016(±0.002)	0.91	0.16351
50	0.284(±0.102)	72	17.6056	0.064(±0.013)	0.91	10.8281	0.008(±0.002)	0.84	0.32703
60	0.708(±0.091)	70	7.0621	0.047(±0.012)	0.87	14.7446	0.005(±0.002)	0.71	0.52326

* C_o and C_t: initial TC concentration and TC concentration at time t (mg/L); t: time (min); k_0, k_1, k_2: kinetic rate constants of zero-, first- and second-order reaction kinetic models.

This investigation is in agreement with other researchers [8,13,50] who explained the Fenton system by the first-order kinetic model. However, some investigators [59–66] indicated that the second-order rate equation fit the kinetic reaction of the photocatalytic oxidation processes.

Referring to the results of the different experimental data at various temperatures (28, 40, 50 and 60 °C), the thermodynamic functions are estimated. The functions include Gibbs free energy of activation (ΔG′), the activation enthalpy (ΔH′), and the activation entropy (ΔS′), which are essential to evaluate the temperature effect on TC oxidation by modified ACBP-Fe_3O_4-based Fenton illumination treatment system. The temperature dependence on the first-order reaction kinetic rate constant of the modified ACBP-Fe_3O_4 Fenton oxidation reaction was estimated through the application of the natural log of ($K = Ae^{\left(\frac{-Ea}{RT}\right)}$) the Arrhenius relation, while the activation energy (Ea) is achieved from the slope of the plot of Figure 11, where k_1 is the kinetic rate constant; Ea is the activation energy (KJ.mol^{-1}); R is the gas constant (8.314 J mol−1 K^{-1}); T is temperature (K) and A is the Arrhenius factor [9,10].

To obtain the Gibbs free energy of activation (ΔG′), Eyring's equation ($k_1 = \frac{k_B T}{h} e^{\left(-\frac{\Delta G^{\#}}{RT}\right)}$) is applied (where k_B and h are Boltzmann and Planck's constants). Additionally, the activation enthalpy (ΔH′) is projected from the equation of $\Delta H' = E_a - RT$ [19,44], and the entropy of activation (ΔS′) is recognized as $\Delta S' = \left(\Delta H' - \Delta G'\right)/T$.

Thermodynamic parameters are investigated and tabulated in Table 6. Negative values of entropy of activation indicate the reduction in the randomness and verify the exothermic tendency of the oxidation system. Further, according to the data displayed in Table 6, the positive Gibbs free energy values suggest that the modified oxidation system has a spontaneous nature. Also, the degree of spontaneity of the oxidation reaction decreases with the increase in temperature. This means the reaction could be induced without being driven by the addition of an external energy source. Since the reaction is exothermic, it releases energy. The overall process was determined to be an exothermic process. These data also support the notion that the proposed t reaction mechanism was energetically stable and that the rate of the Fenton oxidation reaction primarily decreased with the

elevation in temperature, since high temperatures have an opposite influence on the rate of exothermic systems.

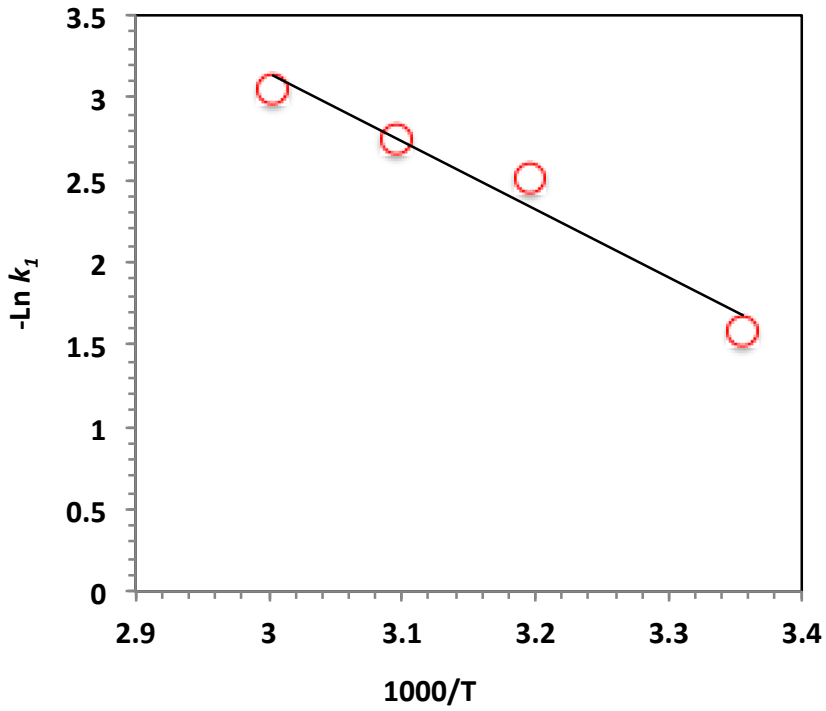


Figure 11. Arrhenius plot of the 1st-order kinetic constants.

Table 6. Thermodynamic parameters for TC oxidation by modified Fenton system.

Temperature, °C	Ln k_1	Ea, kJ mol^{-1}	Δ G′, kJ mol^{-1}	ΔH′, kJ mol^{-1}	ΔS′, J mol^{-1}
28	−1.58	34.3368 (±0.56)	76.914	31.85	−151.17
40	−2.51		83.32	31.73	−164.82
50	−2.74		86.70	31.65	−170.43
60	−3.06		90.33	31.56	−176.45

It is also worth mentioning that the reaction is guided at a low energy barrier of 34.33 kJ/mol. This activation energy value verifies that the reaction slows down with increasing temperature. Previous reports in the literature [9,10] also confirm these findings. Previous researchers reported that the activation energy for dye oxidation by the Fenton reaction is 53.96 kJ/mol [61]. Furthermore, the data tabulated in Table 6 also indicate that ΔS′ exhibited negative values; this indicates that the randomness decreases as a result of the reaction. Randomness in the solution was higher at the beginning of the oxidation reaction compared to the end of the reaction because the reaction rapidly proceeded at the beginning and then slowed down over time.

3.5. Catalyst Sustainability

It is worth examining the sustainability of the catalyst. To this end, the ACBP-Fe_3O_4 catalyst's recover and reuse utility is explored to evaluate its reusability by assessing its activity to ensure its oxidation affinity after use. Primarily, ACBP-Fe_3O_4 is regenerated after magnetic collection and then subsequently subjected to successive distilled water washing. Afterwards, the sample is exposed to oven drying (105 °C) for 1 h. Then, the regenerated catalyst is used as the source of Fenton oxidation and the experiments are conducted under the optimum conditions. The data exhibited in Figure 12 demonstrate the viable efficiency of the material in oxidation, reaching six cyclic uses with a feasible efficiency that decreased from 99% to 90% with successive use.

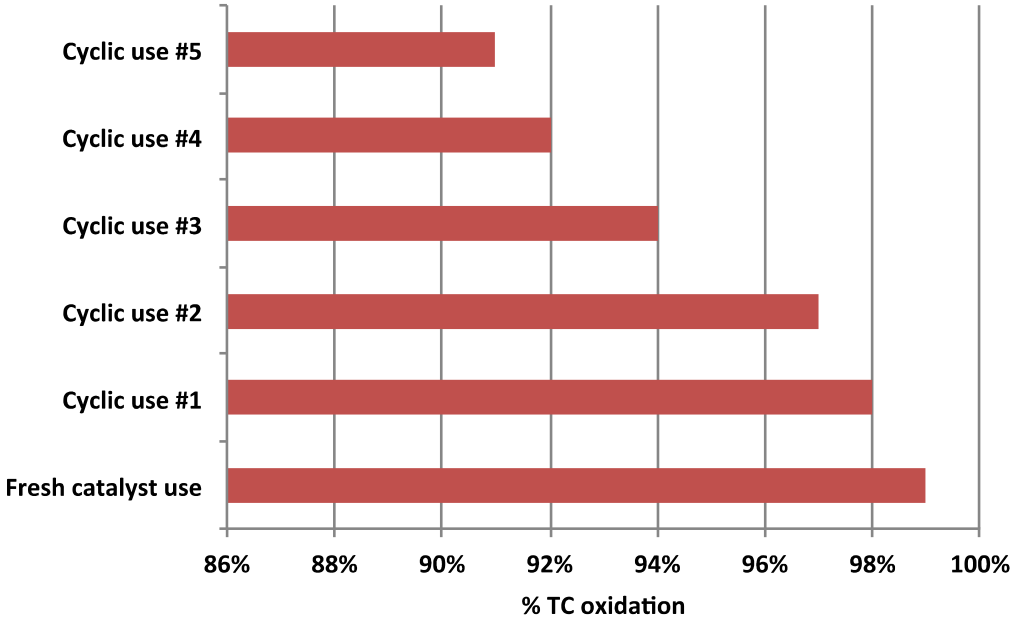


Figure 12. TC oxidation in the Fenton-based ACBP-Fe_3O_4 system in consecutive cycles.

These results could be associated with the occupation of active sites by TC pollutant intermediates, which hinder the activity. However, it is worth mentioning that the ACBP-Fe_3O_4 material still possesses a high oxidation affinity and could be easily recovered.

4. Conclusions

Rapid growth of water contamination is common in current industrial societies and is a growing problem. The use of fruit waste as a precursor for treatment is an industrial ecology approach to substitute the iron source in the classical Fenton's reaction system and could represent a key tool in highlighting the sustainable management of the environment. The removal of tetracycline (TC) as a simulated contaminant from aqueous pharmaceutical discharge is carried out using a modified Fenton reaction based on treated banana peels augmented with magnetite nanoparticles. The removal efficiency reached 98% and 95% for TC and COD removals, respectively. The optimal operational parameters are achieved through response surface numerical methodology, and the optimum oxidation conditions are recorded at H_2O_2 350 mg/L, ACBP-Fe_3O_4 43 mg/L and pH 6.6 with a high correlation coefficient (R^2 0.97%). The temperature effect showed that the reaction is exothermic in nature. The kinetics and thermodynamics of the reaction are also assessed and the reaction follows the first-order reaction kinetics. Consequently, the novel Fenton reagent route from waste could be introduced as a promising green technology for advanced pharmaceutical aqueous effluent oxidation.

Author Contributions: Conceptualization, M.A.T.; Methodology, M.M.N.; Software, M.M.N., M.A.T., H.A.N. and S.M.S.; Formal analysis, M.M.N.; Investigation, H.A.N.; Resources, M.A.T. and S.M.S.; Writing—original draft, M.A.T. and H.A.N.; Writing—review and editing, M.M.N., H.A.N. and S.M.S. All authors have read and agreed to the published version of the manuscript.

Funding: The authors extend their appreciation to Prince Sattam bin Abdulaziz University for funding this research work through the project number (PSAU/2024/01/31504).

Data Availability Statement: Data available upon request.

Conflicts of Interest: The authors declare no conflicts of interest.

References

1. Bahar, M.M.; Mahbub, K.R.; Naidu, R.; Megharaj, M. As(V) removal from aqueous solution using a low–cost adsorbent coir pith ash: Equilibrium and kinetic study. *Environ. Technol. Innov.* **2018**, *9*, 198–209. [CrossRef]
2. Basheer, A.A. Chemical chiral pollution: Impact on the society and science and need of the regulations in the 21st century. *Chirality* **2018**, *30*, 402–406. [CrossRef] [PubMed]
3. Basheer, A.A.; Ali, I. Stereoselective uptake and degradation of (±)-*o*,*p*-DDD pesticide stereomers in water–sediment system. *Chirality* **2018**, *30*, 1088–1095. [CrossRef] [PubMed]
4. Bashir, A.; Malik, L.A.; Ahad, S.; Manzoor, T.; Bhat, M.A.; Dar, G.N.; Pandith, A.H. Removal of heavy metal ions from aqueous system by ion–exchange and biosorption methods. *Environ. Chem. Lett.* **2019**, *17*, 729–754. [CrossRef]
5. Beni, A.A.; Esmaeili, A. Biosorption, an efficient method for removing heavy metals from industrial effluents: A review. *Environ. Technol. Innovat.* **2020**, *17*, 100503. [CrossRef]
6. Bhaumik, R.; Mondal, N.K. Optimizing adsorption of fluoride from water by modified banana peel dust using response surface modelling approach. *Appl. Water Sci.* **2016**, *6*, 115–135. [CrossRef]
7. Tony, M.A.; Lin, L.S. Iron recovery form acid mine drain sludge as a Fenton source for municipal wastewater treatment. *Int. J. Environ. Anal. Chem.* **2020**, *102*, 1245–1260. [CrossRef]
8. Elsayed, S.A.; El-Sayed, I.E.T.; Abdel-Bary, H.M.; Tony, M.A. Chitosan impregnated with magnetite as a versatile photocatalytic nanocomposite for Synozol Red KHL dye elimination from aqueous effluent. *Int. J. Environ. Anal. Chem.* **2023**, *104*, 7871–7897.
9. Tony, M.A.; Mansour, S.A. Microwave-assisted catalytic oxidation of methomyl pesticide by $Cu/Cu_2O/CuO$ hybrid nanoparticles as a Fenton-like source. *Int. J. Environ. Sci. Technol.* **2020**, *17*, 161–174.
10. Tony, M.A.; Zhao, Y.Q.; El-Sherbiny, M.F. Fenton and Fenton-like AOPs for alum sludge conditioning: Effectiveness comparison with different Fe^{2+} and Fe^{3+} salts. *Chem. Eng. Commun.* **2011**, *198*, 442–452.
11. Deng, D.; Lin, L.S. Continuous sulfidogenic wastewater treatment with iron sulfide sludge oxidation and recycle. *Water Res.* **2017**, *114*, 210–217. [PubMed]
12. Pan, W.; Zhang, G.; Zheng, T.; Wang, P. Degradation of p-nitrophenol using CuO/Al_2O_3 as a Fenton-like catalyst under microwave irradiation. *RSC Adv.* **2015**, *5*, 27043–27051.
13. Laureni, M.; Weissbrodt, D.G.; Szivak, I.; Robin, O.; Nielsen, J.; Morgenroth, E.; Joss, A. Activity and growth of anammox biomass on aerobically pre-treated municipal wastewater. *Water Res.* **2015**, *80*, 325–336.
14. Villegas-Guzmana, P.; Giannakis, S.; Rtimi, S.; Grandjeanc, D.; Bensimonc, M.; Alencastro, I.; Torres-Palma, R.; Pulgarin, C. A green solar photo-Fenton process for the elimination of bacteria and micropollutants in municipal wastewater treatment using mineral iron and natural organic acids. *Appl. Catal. B Environ.* **2017**, *219*, 538–549.
15. Van der Zaag, P.J.; Ruigrok, J.J.; Noordermeer, A.; Van Delden, A. The effect of intragranular domain walls in MgMnZn-ferrite. *J. Appl. Phys.* **1993**, *74*, 4085.
16. Wang, S.; Peng, Y. Natural zeolites as effective adsorbents in water and wastewater treatment. *Chem. Eng. J.* **2010**, *156*, 11–24.
17. Thiam, A.; Salazar, R.; Brillas, E.; Sirés, I. In-situ dosage of Fe^{2+} catalyst using natural pyrite for thiamphenicol mineralization by photoelectro-Fenton process. *J. Environ. Manag.* **2020**, *270*, 110835.
18. Poormand, H.; Leili, M.; Khazaei, M. Adsorption of methylene blue from aqueous solutions using water treatment sludge modified with sodium alginate as a low cost adsorbent. *Water Sci. Technol.* **2017**, *75*, 281–295.
19. Saleem, M.; Fang, L.; Ruan, H.B.; Wu, F.; Huang, Q.L.; Xu, C.L.; Kong, C.Y. Effect of zinc acetate concentration on the structural and optical properties of ZnO thin films deposited by sol-gel method. *Int. J. Phys. Sci.* **2012**, *7*, 2971–2979.
20. Srivastava, V.C.; Swamy, M.M.; Mall, I.D.; Prasad, B.; Mishra, I.M. Adsorptive removal of phenol by bagasse fly ash and activated carbon: Equilibrium, kinetics and thermodynamics. *Colloids Surf. A* **2006**, *272*, 89–104.
21. Tiwari, E.M.; Shukla, S.P.; Dhiman, N.; Mohan, D.; Kisku, G.C.; Roy, S. An Efficient Removal of Disperse Dye from Wastewater Using Zeolite. *J. Hazard. Toxic Radioact. Waste* **2017**, *21*, 04017017. [CrossRef]
22. Tong, D.S.; Liu, M.; Lin, C.X.; Yu, W.H.; Zhi, P.X.; Zhou, C.H. Transformation of alunite residuals into layered double hydroxides and oxides for adsorption of acid red G dye. *Appl. Clay Sci.* **2012**, *70*, 1–7.
23. Manera, C.A.; Tonello, P.A.; Perondi, D.; Godinho, M. Adsorption of leather dyes on activated carbon from leather shaving wastes: Kinetics, equilibrium and thermodynamics studies. *Environ. Technol.* **2019**, *40*, 2756–2768. [CrossRef]
24. Doherty, L.; Zhao, Y.Q.; Zhao, X.H.; Wang, W. Nutrient and organics removal from swine slurry with simultaneous electricity generation in an alum sludge-based constructed wetland incorporating microbial fuel cell technology. *Chem. Eng. J.* **2015**, *266*, 74–81.
25. El-Mekkawi, D.M.; Ibrahim, F.A.; Selim, M.M. Removal of methylene blue from water using zeolites prepared from Egyptian kaolins collected from different sources. *J. Environ. Chem. Eng.* **2016**, *4*, 1417–1422.
26. Fungaro, D.A.; Silva, M. Utilization of water treatment plant sludge and coal fly ash in brick manufacturing. *Amer. J. Environ. Prot.* **2014**, *2*, 83–88.

27. Geng, Y.; Zhang, J.; Zhou, J.; Le, J. Study on adsorption of methylene blue by a novel composite material of TiO_2 and alum sludge. *RSC Adv.* **2018**, *8*, 32799–32807. [PubMed]
28. Gomez, S.; Lerici, L.; Saux, C.; Perez, A.L.; Brondino, C.D.; Peirella, L.; Pizzio, L. Fe/ZSM-11 as a novel and efficient photocatalyst to degrade Dichlorvos on water solutions. *Appl. Cata* **2017**, *202*, 580–586. [CrossRef]
29. Jangkorn, S.; Kuhakaew, S.; Theantanoo, S.; Klinla-or, H.; Sriwiriyarat, T. Evaluation of reusing alum sludge for the coagulation of industrial wastewater containing mixed anionic surfactants. *J. Environ. Sci.* **2011**, *23*, 587–594. [CrossRef]
30. Guo, Y.; Xue, Q.; Zhang, H.; Wang, N.; Chang, S.; Wang, H.; Pang, H.; Chen, H. Treatment of real benzene dye intermediates wastewater by the Fenton method: Characteristics and multi-response optimization. *RSC Adv.* **2018**, *8*, 80–90.
31. Bolobajev, J.; Katte, E.; Viisimaa, M.; Go, A.; Trapido, M.; Tenno, T.; Dulova, N. Reuse of ferric sludge as an iron source for the Fenton-based process in wastewater treatment. *Chem. Eng. J.* **2014**, *255*, 8–13. [CrossRef]
32. Pintor, A.M.; Vilar, V.J.; Boaventura, R.A. Decontamination of cork wastewaters by solar-photo-Fenton process using cork bleaching wastewater as H_2O_2 source. *Sol. Energy* **2011**, *85*, 579–587. [CrossRef]
33. Tony, M.A.; El-Gendy, N.S.; Hussien, M.; Ahmed, A.A.S.; Xin, J.; Lu, X.; El-Sayed, I.E.T. Nano-Magnetic Sugarcane Bagasse Cellulosic Composite as a Sustainable Photocatalyst for Textile Industrial Effluent Remediation. *Catalyst* **2024**, *14*, 354. [CrossRef]
34. Bounab, L.; Iglesias, O.; González-Romero, E.; Pazos, M.; Sanroman, M. Effective heterogeneous electro-Fenton process of m-cresol with iron loaded actived carbon. *RSC Adv.* **2015**, *5*, 31049–31056. [CrossRef]
35. Nabwey, H.A.; Tony, M.A.; Nour, M.M. Acetylcellulose recovery from waste residual for attenuating reactive dye from aquaculture waste as a fascinating synergistic ecology effect. *Processes* **2023**, *11*, 2701. [CrossRef]
36. Xu, H.; Li, M.; Miao, J.; Zou, L. Fenton Reagent Oxidation and Decolorizing Reaction Kinetics of Reactive Red SBE. *Energy Procedia* **2012**, *16*, 58–64. [CrossRef]
37. Argun, M.E.; Karatas, E. Application of Fenton process for decolorization of reactive black 5 from synthetic wastewater: Kinetics and thermodynamics. *Environ. Prog. Sus. Ener.* **2011**, *30*, 540–548.
38. Dubber, D.; Gray, N.F. Replacement of chemical oxygen demand (COD) with total organic carbon (TOC) for monitoring wastewater treatment performance to minimize disposal of toxic analytical waste. *J. Environ. Sci. Health* **2010**, *A45*, 1595–1600. [CrossRef]
39. Aziz, J.A.; Tebbutt, T.Y. Significance of COD, BOD and TOC correlations in kinetic–models of biological oxication. *Water Res.* **1980**, *14*, 319–324.
40. Hassan, E.A.; Tony, M.A.; Nabwey, H.A.; Awad, M.M. Potential of the Biomass Waste Originating from Saccharum officinarum as a Fenton Precursor for the Efficient Oxidation of Azo Dye from an Aqueous Stream. *Processes* **2023**, *11*, 1394. [CrossRef]
41. Nabwey, H.A.; Tony, M.A. Distinct pathway of multiferroic silver-decorated zinc ferrite nanocatalyst performance for Acinate insecticide oxidation. *Sci. Rep.* **2024**, *14*, 27078.
42. Yuste-Córdoba, F.J.; Pérez-Salguero, C.; Santiago-Codosero, T.; Godoy-Cancho, B. Improvement of the treatment of cork boiling wastewater by solar photo-Fenton process. *Results Eng.* **2024**, *22*, 102252.
43. Tony, M.A.; Lin, L.S. Attenuation of organics contamination in polymers processing effluent using iron-based sludge. *Environ. Technol.* **2020**, *43*, 718–727. [CrossRef] [PubMed]
44. Zhang, S.; Lia, B.; Wang, X.; Zhao, G.; Hu, B.; Lu, Z.; Wena, T.; Chend, J.; Wang, X. Recent developments of two-dimensional graphene-based composites in visible-light photocatalysis for eliminating persistent organic pollutants from wastewater. *Chem. Eng. J.* **2020**, *390*, 124642.
45. Shende, T.P.; Bhanvase, B.A.; Rathod, A.P.; Pinjari, D.V.; Sonawane, S.H. Sonochemical synthesis of Graphene-Ce-TiO_2 and Graphene-Fe-TiO_2 ternary hybrid photocatalyst nanocomposite and its application in degradation of crystal violet dye. *Ultrason. Sonochem.* **2018**, *41*, 582–589.
46. Bosio, G.N.; García Einschlag, F.S.; Carlos, L.; Mártire, D.O. Recent Advances in the Development of Novel Iron–Copper Bimetallic Photo Fenton Catalysts. *Catalysts* **2023**, *13*, 159. [CrossRef]
47. Lai, Y.J.; Lee, D.J. Solid Mediator Z–Scheme Heterojunction Photocatalysis for Pollutant Oxidation in Water: Principles and Synthesis Perspectives. *J. Taiwan Inst. Chem. Eng.* **2021**, *125*, 88–114.
48. Zolfaghari, G.; Esmaili-Sari, A.; Anbia, M.; Younesi, H.; Ghasemian, M.B. A zinc oxide-coated nanoporous carbon adsorbent for lead removal from water: Optimization, equilibrium modeling, and kinetics studies. *Int. J. Environ. Sci. Technol.* **2013**, *10*, 325–340.
49. Joshi, S.; Garg, V.K.; Kataria, N.; Kadirvelu, K. Applications of Fe_3O_4@ AC nanoparticles for dye removal from simulated wastewater. *Chemosphere* **2019**, *236*, 124280.
50. Zhang, M.H.; Dong, H.; Zhao, L.; Wang, D.-X.; Meng, D. A Review on Fenton Process for OrganicWastewater Treatment Based on Optimization Perspective. *Sci. Total Environ.* **2019**, *670*, 110–121.
51. Abdollahzadeh, H.; Fazlzadeh, M.; Afshin, S.; Arfaeinia, H.; Feizizadeh, A.; Poureshgh, Y.; Rashtbari, Y. Efficiency of activated carbon prepared from scrap tires magnetized by Fe_3O_4 nanoparticles: Characterisation and its application for removal of reactive blue19 from aquatic solutions. *Int. J. Environ. Anal. Chem.* **2020**, *102*, 1911–1925. [CrossRef]

52. Tony, M.A.; Ali, I.A. Mechanistic implications of redox cycles solar reactions of recyclable layered double hydroxides nanoparticles for remazol brilliant abatement. *Int. J. Environ. Sci. Technol.* **2021**, *19*, 9843–9860. [CrossRef]
53. Maroudas, A.; Pandis, P.K.; Chatzopoulou, A.; Davellas, L.-R.; Sourkouni, G.; Argirusis, C. Synergetic decolorization of azo dyes using ultrasounds, photocatalysis and photo-fenton reaction. *Ultrason. Sonochem.* **2021**, *71*, 105367. [CrossRef] [PubMed]
54. Huang, X.; Nan, Z. Formation of octahedron-shaped $ZnFe_2O_4/SiO_2$ with yolk–shell structure. *J. Phys. Chem. Solids* **2020**, *141*, 109410. [CrossRef]
55. Channei, D.; Thammaacheep, P.; Jannoey, P. Utilizing banana peel in conjunction with TiO_2 photocatalyst for the efficient decolorization of malachite green. *Chem. Phys. Impact.* **2024**, *8*, 100629. [CrossRef]
56. Eskandari, P.; Farhadian, M.; Solaimany Nazar, A.R.; Goshadrou, A. Cyanide adsorption on activated carbon impregnated with ZnO, Fe_2O_3, TiO_2 nanometal oxides: A comparative study. *Int. J. Environ. Sci. Technol.* **2021**, *18*, 297–316. [CrossRef]
57. Hami, H.K.; Abbas, R.F.; Eltayef, E.M.; Mahdi, N.I. Applications of aluminum oxide and nano aluminum oxide as adsorbents: Review. *Samarra J. Pure Appl. Sci.* **2021**, *2*, 19–32. [CrossRef]
58. Serna-Jimenez, J.A.; Luna-Lama, F.; Caballero, A.; Martín, M.A.; Chica, A.F.; Siles, J.A. Valorisation of banana peel waste as a precursor material for different renewable energy systems. *Biomass Bioenerg.* **2021**, *155*, 106279. [CrossRef]
59. Abdel-Khalek, A.; Hamed, A.; Hasheesh, W. The Potential Use of Orange and Banana Peels to Minimize the Toxicological Effects of Silver Nanoparticles in Oreochromis Niloticus. *Bull. Environ. Contam. Toxicol.* **2022**, *108*, 985–994.
60. Ozmen, M.; Can, K.; Arslan, G.; Tor, A.; Cengeloglu, Y.; Ersoz, M. Adsorption of Cu (II) from aqueous solution by using modified Fe_3O_4 magnetic nanoparticles. *Desalination* **2010**, *254*, 162–169. [CrossRef]
61. Singh, C.; Rubina Chaudhary, R.; Gandhi, K. Preliminary study on optimization of pH, oxidant and catalyst dose for high COD content: Solar parabolic trough collector. *Iran J. Environ. Health Sci. Eng.* **2013**, *10*, 13–23. [CrossRef] [PubMed]
62. Lopez-Lopez, C.; Martin-Pascual, J.; Martınez-Toledo, M.V.; Gonzalez-Lopez JHontoria, E.; Poyatos, J.M. Effect of the operative variables on the treatment of wastewater polluted with Phthalo Blue by H_2O_2/UV process. *Water Air Soil Poll.* **2013**, *224*, 1725. [CrossRef]
63. Fu, X.; Clark, L.A.; Zeltner, W.A.; Anderson, M.A. Effects of reaction temperature and water vapor content on the heterogeneous photocatalytic oxidation of ethylene. *J. Photochem. Photobiol. A Chem.* **1996**, *97*, 181–186. [CrossRef]
64. Soares, E.T.; Lansarin, M.A.; Moro, C.C. A study of process variables for the photocatalytic degradation of Rhodamine B. *Braz. J. Chem. Eng.* **2007**, *24*, 29–36.
65. Buthiyappan, A.; Raman, A.; Daud, W. Development of an advanced chemical oxidation wastewater treatment system for the batik industry in Malaysia. *RSC Adv.* **2016**, *30*, 25222–25241. [CrossRef]
66. Lan, B.Y.; Nigmatullin, R.; Puma, G.L. Ozonation kinetics of cork- processing water in a bubble column reactor. *Water Res.* **2008**, *42*, 2473–2482. [CrossRef] [PubMed]
67. Lucas, M.S.; Mosteo, R.; Maldonado, M.I.; Malato, S.; Peres, J.A. Solar photochemical treatment of winery wastewater in a CPC reactor. *J. Agric. Food Chem.* **2009**, *57*, 11242–11248. [CrossRef]
68. Ho, Y.S.; Ng, J.C.Y.; Mckay, G. Kinetics of pollutant sorption by biosorbents: Review. *Seperation Purif. Method* **2000**, *29*, 189–232.
69. Ahmadi, M.; Behin, J.; Mahnam, A.R. Kinetics and thermodynamics of peroxydisulfate oxidation of Reactive Yellow 84. *J. Saudi Chem. Soci.* **2016**, *20*, 644–650.
70. Caballero, A.; Hern'an, L.; Morales, J. Limitations of disordered carbons obtained from biomass as anodes for real lithium-ion batteries. *ChemSusChem* **2011**, *4*, 658–663.
71. Muthukannan, V.; Praveen, K.; Natesan, B. Fabrication and characterization of magnetite/reduced graphene oxide composite incurred from iron ore tailings for high performance application. *Mater. Chem. Phys.* **2015**, *162*, 400–407.
72. Hilder, M.; Winther-Jensen, O.; Winther-Jensen, B.; MacFarlane, D.R. Graphene/zinc nano-composites by electrochemical co-deposition. *Phys. Chem. Chem. Phys.* **2012**, *14*, 14034–14040. [PubMed]

Disclaimer/Publisher's Note: The statements, opinions and data contained in all publications are solely those of the individual author(s) and contributor(s) and not of MDPI and/or the editor(s). MDPI and/or the editor(s) disclaim responsibility for any injury to people or property resulting from any ideas, methods, instructions or products referred to in the content.